Vibration Suppression of Large Deployable Space Structures Based on Viscous Damping

Min Luo[a,b], Zheng H. Zhu[c,*], Qinghua Xu[a], Yaobin Wang[a,b], Wenbo Luo[a,b]

a Beijing Institute of Spacecraft System Engineering, Beijing 100094, PR China

b Beijing Key Laboratory of Intelligent Space Robotic System Technology and Applications, Beijing 100094, China

c Department of Mechanical Engineering, York University, M3J 1P3, Canada

Abstract

This paper proposes an optimal design strategy for the vibration suppression system of large deployable space structures, which is critical for space mission because there is no sufficient damping in such space structures. Viscous dampers are commonly employed to suppress the vibration due to their simple design, low cost, and stable damping performance. However, the harsh space environment makes the normal viscous dampers suspicious to various failures. A novel and robust design of viscous damper is developed in the current work to provide high damping under low-frequency vibration disturbance in space. The characterization of the newly developed damper at low-frequency and large displacement is first investigated by numerical analysis and then validated by experiments. The design is further optimized by weighted-sum that includes the damping characteristics of dampers and elastic flexibility of space structures – space trusses. The effect of vibration suppression by the proposed dampers and their placement in structures is demonstrated by the optimal design of a 60-meter deployable truss. The results show that the damping ratios of the first three modes of the deployable truss can be increased by over 10% with two viscous dampers. Comparisons between the structure with and without dampers demonstrate that significant vibration suppression at low-frequency bandwidth can be achieved satisfactorily.

Keywords: space structures, vibration suppression, viscous damper, weighted-sum optimization

1 Introduction

Improvements of aerospace science and technology in the field of telecommunications, earth observation, space telescope, and space stations intensify the demand for large-dimension and high-precision space structures. As astrophysics missions are reaching the limits of the launchers' capabilities, large deployable space structures which can be transformed from a compact folded state to anticipatory deployed form are widely used [1]. For some kinds of space crafts, such as Synthetic Aperture Radars (SAR) [2], Interferometric Imaging Telescopes[3], and Reflective Imaging Space Telescopes [4], increasing apertures or increasing baselines and focal lengths are the main solutions to improve the imaging accuracy. That means larger surface or length of deployable structures [5]. However, due to their big size and lightly damped nature modal, large deployable structures are easily vibrated by a minor disturbance on orbit and difficulty suppressed. Thus, with the trend of large-aperture and light-weight future astrophysics missions, flexible low-frequency vibration control of large deployable structures becomes one of the most important challenges that may influence the missions. Therefore, the requirements for deployable space structures are not only the deploying precision but also the stability, that is to say, the flexible vibration of structures should be restrained rapidly to avoid the influence to the satellite [6].

There are numerous works have been published on vibration suppression of large deployable space structures which can be mainly categorized as active control and passive suppression. Active vibration control strategy has been successfully implemented for vibration attenuation of beams, plates, and shells by numerous researchers [7]. Although active approaches are very attractive and to be considered as the development trends in vibration suppression for flexible space structures. They need sensors to measure the level of vibration, controllers to process the sensor signals and send driving signals, drivers to apply forces to reduce the vibration, which are more complicated and costly than passive methods. In addition, active systems require power for operating the

* Corresponding author. Tel: (416) 7362100 x 77729

E-mail address: gzhu@yorku.ca

sensors, controllers, and drivers. On the other hand, passive damping technology introduces high damping materials such as viscous damping [8], viscoelastic damping [9], etc. into the structures to improve the modal damping in vibration motion. Passive vibration control systems function without external service, and they are driven by the vibration itself, so not require power. They require little or no maintenance, and installation is relatively simple and low cost. Therefore, it is commonly applied passive damping approach for vibration suppression of large deployable space structures at present.

Viscous damping is one of the common applications of passive damping systems according to its simple configuration, low cost, and stable damping. It was first used in the Hubble telescope to isolate micro-vibrations from reaction wheel [10]. Taylor devises inc. has developed a series of hermetically sealed fluid dampers [11]. In 2000, two viscous damping mechanisms were applied for the Shuttle Rader Topography Mission (SRTM) [12].

The critical part in designing such a viscous damping system is to demonstrate the damping characteristics of viscous dampers as realistic as possible and introduce the damping elements into the structural systems efficiently. In this paper, a viscous damper is proposed, which can provide high damping under low-frequency vibration loading. The numerical investigations were carried out to study the performance of such a viscous damping methodology. Based on the indicator diagram method, the damping ratio of the viscous damper was tested on the damping test bed, which agrees well with the numerical analysis. Furthermore, a weighted-sum optimization algorithm including the damping characteristics of dampers and flexible numerical model of space structures is presented to place passive viscous dampers in space trusses. Finally, an example of adding damping system into a 60-meter deployable truss is presented to show how to use the damping analysis and the optimization algorithm for vibration suppression of the large deployable space structures.

2 Viscous damper design and analysis

2.1 Viscous damper design

Fig. 1 shows the internal configuration of a viscous damper. Ball joints on each side of the damper are used to attach to the external objects. A central piston rod strokes through the fluid-filled chamber A and chamber B. The piston rod moves right and left with respect to the cylinder. As the piston rod moves it pushes fluid through a gap between the piston head and the cylinder. Fluid velocity is very high in this region so pressure loss develops as a result of the shearing action of the silicone fluid. Due to the pressure loss, there is very little pressure on the downstream side of the piston head compared with the full pressure on the upstream side of the piston head. This difference in pressures produces a large damping force that resists the motion of the damper. Labyrinth frictionless seals are applied to seal the fluid in the chambers instead of O-ring seals or other contact seals. So, there is nothing to wear out or deteriorate over time. Silicone oil is used due to its long-term stability and lower sensitivity with temperature changes. All these approaches can be expected to obtain a long-life and stable viscous damper.

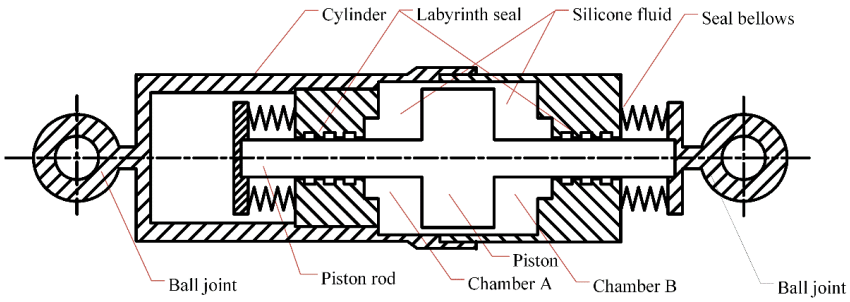

Fig. 1. Schematic of a viscous damper

2.2 Numerical analysis of the damper

Fluent in the commercial finite-element package ANSYS is used to calculate the fluid dynamics in the damper. To simplify the analyses, the silicone oil is assumed to be Newtonian and incompressible with a density of 0.94 g/cm^3 and a viscosity of 20 cSt. A two-dimensional axisymmetric flow simplified model is adopted to reduce computation due to a completely

axisymmetric flow of the silicone oil in the damper. The finite-element model of the damper is shown in Fig. 2. Flow regions combine with the chamber A, chamber B, labyrinth seals and seal bellows in Fig. 1, where are filled with the silicone oil. The piston is moved according to a simple harmonic motion. The moving equation is,

$$x(t) = A\sin(2\pi ft) \quad (1)$$

Here, x is the displacement of the piston, A is the amplitude, and f is the frequency. During the calculation process, the pressure of seal bellows is constant as a simplified boundary condition. The RANS equation and a Realizable k-ε turbulence model is considered to solve the model. Finite volume method is used to discrete the governing equations.

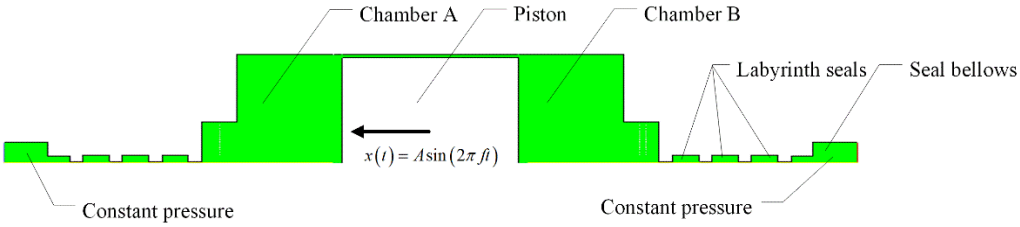

Fig. 2. Finite-element model of the viscous damper

Fig. 3 shows the simulation results of the streamline distribution of flow field in half cycle of piston motion. It can be found the fluid velocity increases very rapidly through the gap between the piston and the cylinder. When the fluid subsequently expands into the other side of the piston it forms an obvious vortex. The vortex slows down the fluid velocity and absorbs kinetic energy into internal energy of the silicone oil.

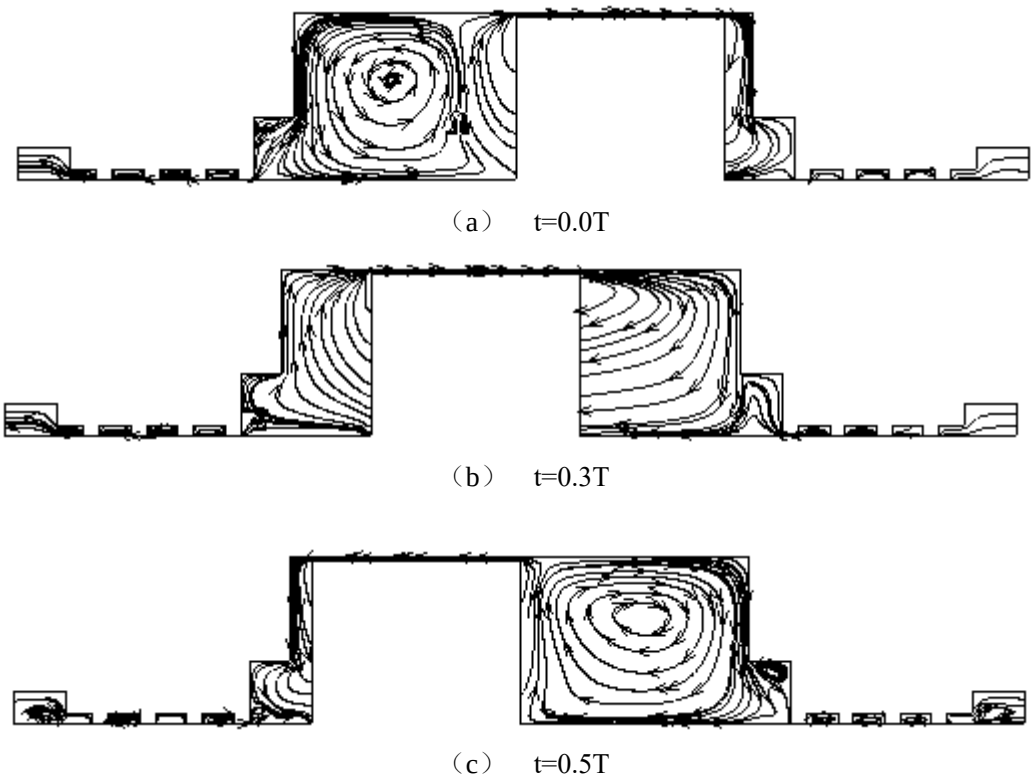

Fig. 3. Streamline distribution of flow field in half cycle of the piston motion (T is the time of a cycle of sine motion of the piston)

The axis force of the piston, D, is recorded at each time step from the calculation results. Based on the relationship of the time to the displacement of piston, the force-displacement curve of a complete cycle of the piston motion (A=1mm and f=1Hz) is shown in Fig. 4, which is a type of elliptical curve named indicator diagram, as shown in Fig. 4. The damping ratio of the damper can be calculated from the indicator diagram by the equation as

$$\bar{c} = \frac{\oint D dx}{2\pi^2 A^2 f} \quad (2)$$

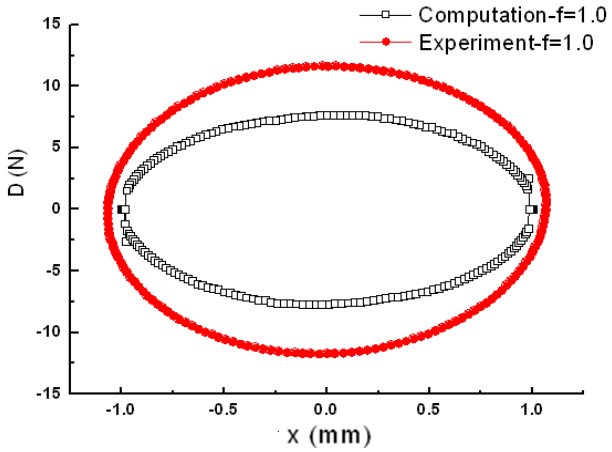

Fig. 4. Comparison of numerical and experimental indicator diagram of the damper (A=1mm and f=1Hz)

A series of simulation conditions with different piston motion A=1, 3, and 5mm, f=0.05, 0.5, 1, 1.5, 2, and 2.5Hz have been calculated. As a result, the damping ratios against the frequency, for the amplitude of displacement A=1, 3, and 5mm are shown in Fig. 5. The damping ratio increases almost linearly with the frequency. The amplitude of displacement also has a significant effect on the damping ratio. It is clear that for larger values of A higher values of the damping ratio are outputted by the damper. In conclusion, the damping characteristic shown in Fig. 5 can help us to build accurate damping elements in the applications of damping systems, which will be shown in the following chapter.

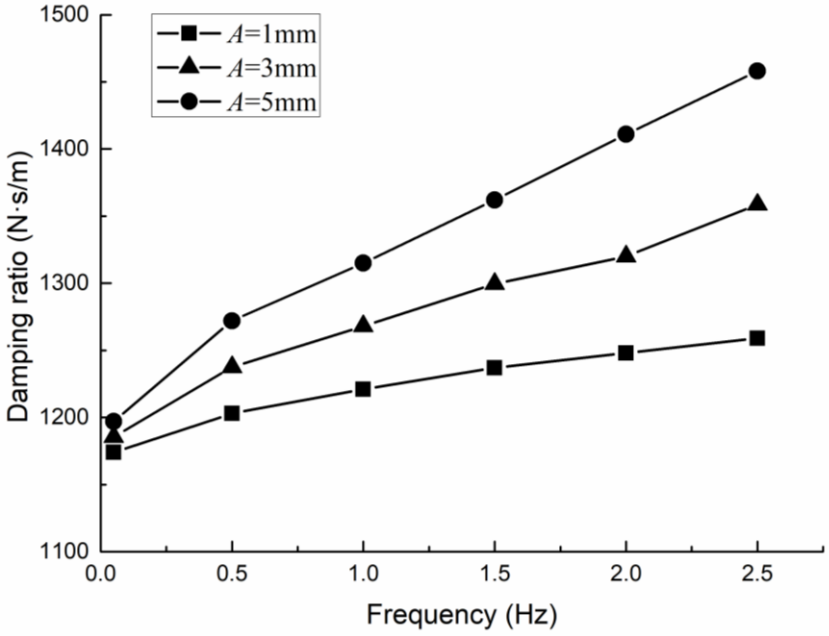

Fig. 5. Plot of the damping ratios, $\bar{c}$, against the frequency, f, for A=1, 3, and 5mm.

2.3 Experiments of the damper

To validate the damping ratios of the viscous damper calculated by the numerical analysis, damping tests were performed. Fig. 6 shows the damping test setup configuration on the damper testbed. A viscous damper, which was manufactured in accordance with the design shown in Fig.1 and was the same as the numerical model in Fig. 2, was tested on the damper testbed. A single axis load cell was set on a steel wall of steel frame and connected with the piston head of damper. A hydraulic actuator was tightly attached to the cylinder of damper. Because the piston head was fixed without motion, the actuator motion could be used to describe the motion of damper. The

displacement of the actuator was measured by a displacement sensor in the actuator head. Sinusoidal displacements with frequencies, *f*, of 0.5 to 2.5Hz were applied and the displacement amplitude, *A*, was 1 mm in each test. The force-displacement curves, that are, the experimental indicator diagrams of the damper, were obtained during the tests. Using the same method shown in section 2.2, the damping ratios can be calculated from the experimental indicator diagrams.

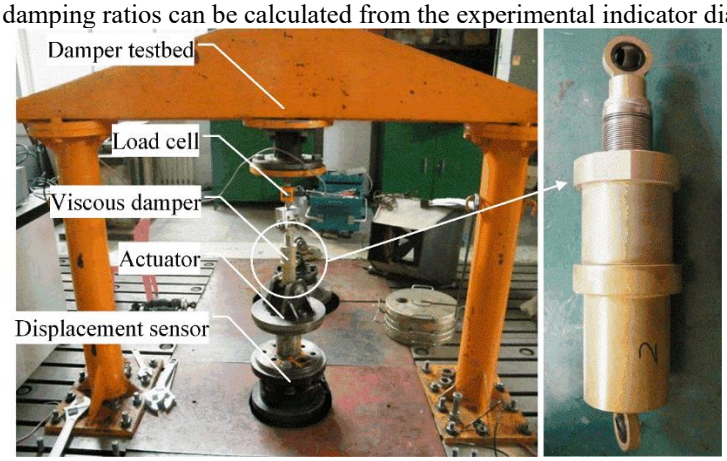

Fig. 6. Setup of damper tests

Fig. 4 illustrates experimental and numerical force-displacement curves in the case of A=1mm and f=1Hz and a larger elliptical curve is obtained from the experiment. Fig. 7 shows the damping ratios in the cases of A=1mm and f=0.5, 1, 1.5, 2, and 2.5Hz. The experimental damping ratio increases linearly with the frequency and the slope of the curve is almost the same as the numerical result. The damping ratio obtained from the tests is about 11% higher than that in numerical simulations. One possible reason for this difference is that the friction damping caused by the motion of the actuator is introduced into the load cell which was not simulated in the numerical analysis.

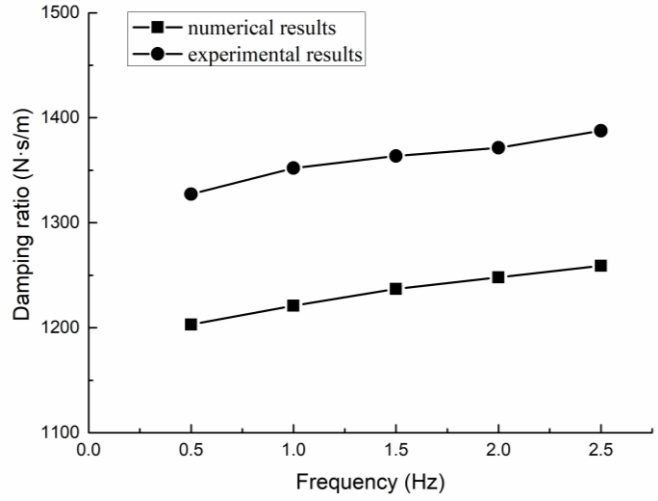

Fig. 7. Comparison of experimental and numerical damping ratios against with the load frequency (A=1mm).

3 Vibration suppression of large deployable space structures

3.1 Description of a weighted-sum optimization algorithm

Large deployable space structures represent a practical spacecraft problem. Thruster firings, thermal strains, and other factors can easily induce vibrations detrimental to payloads. The performance of payloads will be degenerated by the position, orientation change due to vibrations. In this case, the suppression of the resulting vibrations is necessary. Viscous damper presented in this paper is an ideal method for its simplicity and amenability to analysis tools. However, the optimal design of the damping application has several challenges. For example, the behavior of an assembled truss structure will often be nonlinear. The number of dampers is often limited by the economic and

engineering costs, and the positions can be used to add the dampers are usually restricted by the deployment requirement of the structure. To optimize a design successfully with these limits and freedoms, a weighted-sum optimization algorithm is proposed in this study. This optimization technique has been employed to enhance the damping ratios of the deployable structures in a wide frequency range including various nature modes. The basic procedure is outlined in Fig. 8.

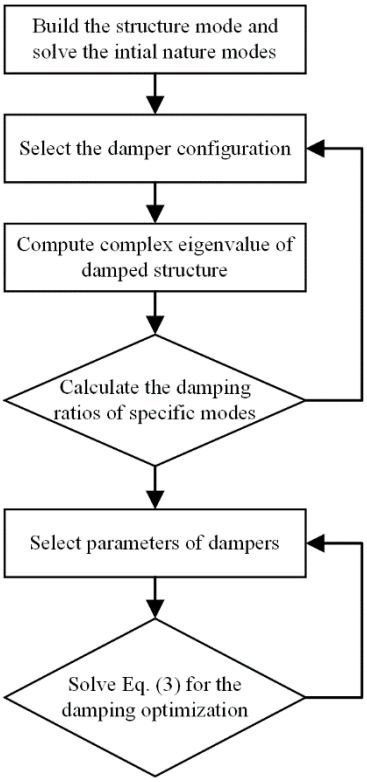

Fig. 8. Optimization algorithm flowchart

Each design starts from a nature mode analysis by a numeral model of an undamped structure. The NASTRAN code is usually used to build the structure model and solve natural modes of the deployed structure. The kinetic and strain energy remaining in the structure are evaluated, which will help us to understand the range of choice to set up the dampers.

After the entire undamped modes are evaluated, various optional damper configurations are introduced into the model. The viscous dampers are simplified as functional damping elements with the damping characteristic described in chapter 2. By complex characteristic value evaluation of the damped structure model, the damping ratios of nature modes can be solved. An optimization process is conducted to find out the best damper configuration and ensure that all of the specific nature modes will be damped.

Our algorithm next selects parameters of the dampers for the specific damper configuration by a weighted-sum optimization method. An optimal cycle is applied to find the maximum value of weighted-sum optimization function by changing the parameters of dampers. The equation of the weighted-sum optimization function is expressed in the frequency domain as:

$$J = \sum_{i=1}^{m} a_i \eta_i \quad (3)$$

Where a_i is the weighted factor of i-order mode; η_i is the damping ratio of *i*-order mode and m is the number of modes in the calculated range of frequency domain. a_i is determined by the vibration suppression requirement of the payload. For example, a typical application of large deployable space structure, Interferometric Synthetic Aperture Radar (InSAR) is widely used in geodesy and remote sensing. This geodetic method uses two or more synthetic aperture radar (SAR) images to generate maps of surface deformation or digital elevation, using differences in the phase of waves returning to the satellite [14]. Due to the image principle of InSAR, weighted factors of the bending modes of the deployable mast are high, and weighted factors of the torsional modes of the deployable mast are low, according to large relative displacements of the two synthetic aperture radar in the bending modes.

Through the optimization algorithm flowchart, the number, the places, and the directions of dampers can be determined to ensure optimal damping increasing in specific nature modes of deployable

space structures. This optimization technique would be employed to solve a wide variety of problems in the fields of space structural dynamics and system optimization.

3.2 Example of application on deployable truss masts

A typical kind of large deployable space structure, deployable truss mast, is used to validate proper operation of the viscous damping method and the optimization algorithm in this chapter. This kind of structure contains a number of pinned joints and allows creating deployable lightweight masts extending up to several tens of meters. Sever such masts have been applied, such as the JXAX masts used to achieve 12m focal length necessary for Hard X-ray Imager on ASTRO-H mission in 2013 [15], or the American deployable articulated mast (ADAM) applied for extensions up to 60m for shuttle radar topographic mission (SRTM) in 1999 [13]. For instance, the ADAM mast can take 360-kg outboard antenna at its end and deploy from its canister to 60 meters in space, with eigenfrequency about 0.05Hz. However, the first eigenfrequency of ADAM is quite low. A mast vibration damping subsystem should be implemented in order to meet dynamic control requirements of ADAM.

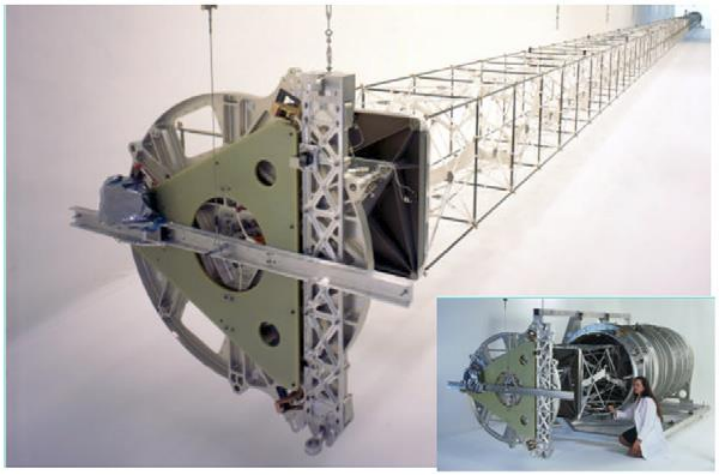

Fig. 9. The ADAM mast deployed and canister (adapted from [13]).

Following the first step in Fig. 8, a finite element model (FEM), which consists of a 60-meter truss, a canister fixed at one end of the truss, and an outboard antenna attached at the other end of the truss, is shown in Fig. 10. The primary structural members of the 60-meter truss are 60 segments of longerons. Each longeron is made from 5A06-T6 aluminum and is simulated by a beam element in the FEM. Each longeron segment is 1 meter long from end to end, and the overall 60-bay mast is 60 meters in length. The outboard antenna is simplified as a 360-kg lumped mass, which is attached at the end of the mast by MPC elements. The canister is made from 5A06-T6 aluminum, which is modeled by shell elements. The structural attachment of the mast, via the canister, to the main structure of the spacecraft, is shown in Fig. 10, which serves to attach the mast system to the main body of the spacecraft. The structural attachment consists of 3 rigid struts and 2 damper struts. The front 2 rigid struts are fixed with the canister. The behind rigid strut and the 2 damper struts are connected with the canister by universal couplings. All of the struts are fixed on the main struct of the satellite by spherical bearings. As a result, the vibration of the entire deployed mast is transferred to the rotates of the canister as a rigid body, which is controlled by the motion of the struts. The dampers located in the struts control the respective vibration modes of the mast due to their locations.

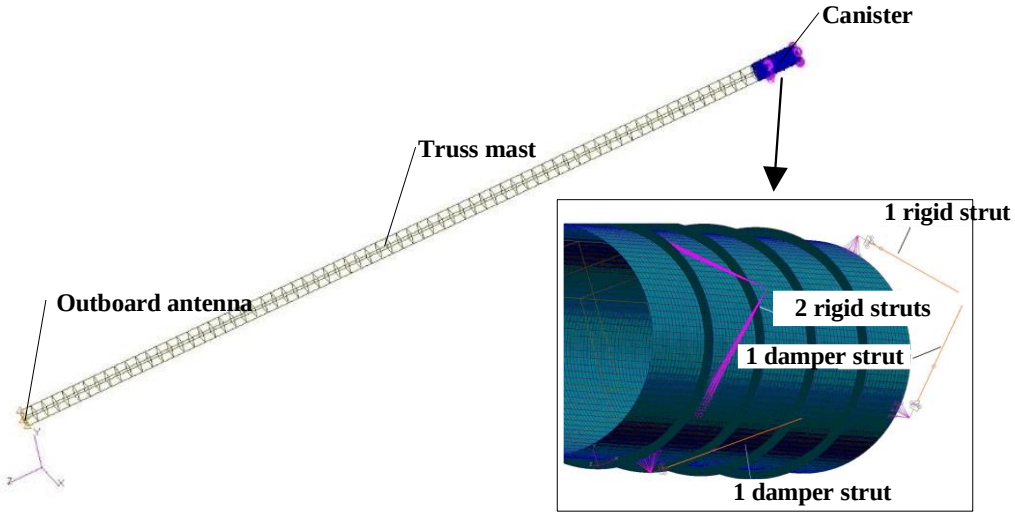

Fig. 10. Finite element model of 60-meter deployable truss mast system and canister attachment struts.

Three damper configurations illustrated in Fig. 11 are taken into the finite element model. Comparing configuration A with configuration B, the direction of the front damper strut is changed. Locations of the behind struts are moved forward from configuration B to configuration C. The same initial damping ratios of dampers are used in the three configurations. Table 1 shows simulated modal damping ratios of the mast in the three damper configurations. It can be found that configuration B provides a uniform damping of the first four modes and a relatively high frequency.

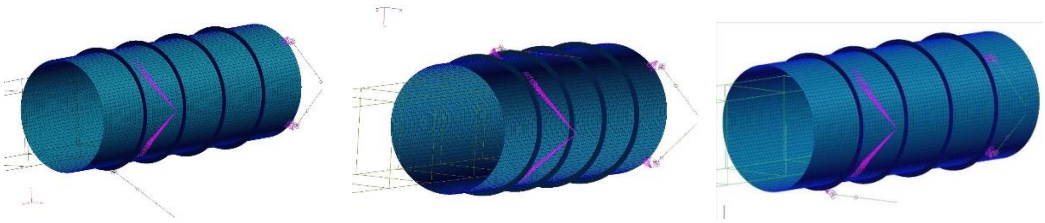

(a) Configuration A (b) Configuration B (c) Configuration C

Fig. 11. Three damper configurations for the optimization

Table 1. Mode damping ratios of damper configurations

Mode	Configuration A		Configuration B		Configuration C	
	Frequency (Hz)	Damping ratio	Frequency (Hz)	Damping ratio	Frequency (Hz)	Damping ratio
1	0.04	5.92%	0.04	5.84%	0.03	4.70%
2	0.12	2.89%	0.11	6.02%	0.08	5.22%
3	0.23	13.00%	0.22	7.12%	0.21	6.98%
4	0.44	10.64%	0.42	3.84%	0.43	4.17%

As mentioned above, parameters of the dampers are optimized by the weighted-sum optimization method after we choosing Configuration B. Weighted factors of the first four modes are proposed in Table 2. The first mode and the second mode are X-direction bending mode and Y-direction bending mode respectively, which have a serious impact on the precision of payload. Thus, weighted factors of the first mode and the second mode are 0.9. The third mode is the torsion mode, which has a light impact on the precision of payload. The weighted factor is 0.7. The fourth mode is the second order of bending mode, the displacement of the tip of the mast is very small in this vibration mode and the weighted factor is 0.3. Optimal cycles are applied to find the maximum value of the weighted-sum optimization function according to Eq. (3). After several cycles, the weighted-sum optimization function, J, is increased from 0.17 to 0.35, and the damping ratio of the first three modes are increased above 10%.

Table 2. Comparison of computation results before and after optimization

Mode	weighted factor	Before optimization		After optimization	
		Frequency (Hz)	Damping ratio	Frequency (Hz)	Damping ratio
1	0.9	0.04	5.84%	0.04	11.75%
2	0.9	0.11	6.02%	0.11	11.92%
3	0.7	0.22	7.12%	0.24	15.09%
4	0.3	0.42	3.84%	0.41	7.58%

To validate the vibration suppression of the damping system after the optimization, a group of frequency response analysis was conducted. The comparison of Tip displacement responses in the frequency domain for damped and undamped masts is demonstrated in Fig. 12. It can be found that the tip displacement of the mast is suppressed obviously after the damping system setup into the system. In other words, the result shows that the damping system effectively reduces the vibration of the mast.

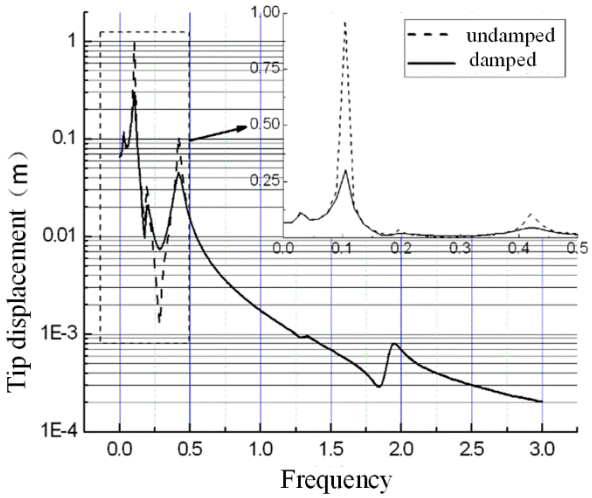

Fig. 12. Tip displacement versus frequency for damped and undamped masts

4 Conclusions

This paper presents a novel and robust design of viscous damper to provide high damping under low-frequency vibration disturbance in space. The damping characteristics of dampers are calculated by the fluid dynamics numerical analysis and then validated by experiments. After that, the paper proposes a robust design method of a passive viscous damping system to suppress the flexible vibration of large deployable space structures. A useful optimization algorithm flowchart has been developed. The method used a weighted-sum optimization function to allow the designer to easily take into account the impact degrees of different frequency modes.

In order to understand more clearly the design process of the damping system, an example of the damping system design for a 60-meter deployable truss is demonstrated. The results show that the damping ratios of the first three modes of the deployable truss can be increased by over 10% with two viscous dampers. Comparisons between the structure with and without dampers demonstrate that significant vibration suppression at low-frequency bandwidth can be achieved satisfactorily.

References

[1]. Kiper G, Soylemez E. Deployable space structures[C]//2009 4th International Conference on Recent Advances in Space Technologies. IEEE, 2009: 131-138.

[2]. Bamler R, Hartl P. Synthetic aperture radar interferometry[J]. Inverse problems, 1998, 14(4): R1.

[3]. Beckers J M. Interferometric imaging with the very large telescope[J]. Journal of Optics, 1991,

22(2): 73-83.
[4]. Sabelhaus P A, Decker J E. AN overview of the James Webb Space Telescope (JWST) project[C]//Optical, Infrared, and Millimeter Space Telescopes. International Society for Optics and Photonics, 2004, 5487: 550-564.
[5]. Puig L, Barton A, Rando N. A review on large deployable structures for astrophysics missions[J]. Acta Astronautica, 2010, 67(1-2): 12-26.
[6]. Zhang Y, Yang D, Li S. An integrated control and structural design approach for mesh reflector deployable space antennas[J]. Mechatronics, 2016, 35: 71-81.
[7]. Sharma A, Kumar R, Vaish R, et al. Active vibration control of space antenna reflector over wide temperature range[J]. Composite Structures, 2015, 128: 291-304.
[8]. Lee D, Taylor D P. Viscous damper development and future trends[J]. The Structural Design of Tall Buildings, 2001, 10(5): 311-320.
[9]. Zhou X Q, Yu D Y, Shao X Y, et al. Research and applications of viscoelastic vibration damping materials: a review[J]. Composite Structures, 2016, 136: 460-480.
[10]. Davis L P, Cunningham D, Bicos A S, et al. Adaptable passive viscous damper: an adaptable D-StrutTM[C]//Smart Structures and Materials 1994: Passive Damping. International Society for Optics and Photonics, 1994, 2193: 47-59.
[11]. https://www.taylordevices.com/.
[12]. Umland J W. SRTM mast damping subsystem design and failure investigation[J]. 2001.
[13]. Umland J, Eisen H. SRTM on-orbit structural dynamics[C]//19th AIAA Applied Aerodynamics Conference. 2001: 1588.
[14]. Massonnet D, Feigl K L. Radar interferometry and its application to changes in the Earth's surface[J]. Reviews of Geophysics, 1998, 36(4): 441-500.
[15]. Takahashi T, Mitsuda K, Kelley R, et al. The ASTRO-H x-ray observatory[C]//Space Telescopes and Instrumentation 2012: Ultraviolet to Gamma Ray. International Society for Optics and Photonics, 2012, 8443: 84431Z.